CrossMark

Determination of NEHRP Site Class of Seismic Recording Stations in the Northwest Himalayas and Its Adjoining Area Using HVSR Method

N. H. Harinarayan[1] and Abhishek Kumar[1]

Abstract—Local site characteristics play an important role in controlling the damage pattern during earthquakes (EQs). These site characteristics may vary from simple to complex and can be estimated by various field tests. In addition, extended Nakamura's method, which uses horizontal to vertical spectral ratio (HVSR) based on available EQ records also available for site class (SC) determination. In this study, SCs for 90 recording stations which are maintained by Program for Excellence in Strong Motion Studies (PESMOS), located in the northwestern Himalayas and the adjoining areas are determined using extended Nakamura's technique. Average HVSR curves obtained at majority of the recording stations are found matching with the existing literature. Predominant frequency (f_{peak}) from average HVSR curve at each recording station is then used for the determination of SC. Original SC given by PESMOS is purely based on geology and not based on comprehensive soil investigation exercise. In this study, the SC, which is based on the average HVSR curves is found matching with SC given by PESMOS for a majority of recording stations. However, for considerable number of recording stations, a mismatch is also found which is consistent with the existing literature. In addition, SC based on National Earthquake Hazard Reduction Program (NEHRP) scheme is proposed based on f_{peak} for all the 90 recording stations.

Key words: Local soil, PESMOS, site classification, northwest himalayas, HVSR.

1. Introduction

The characteristics of surface ground motion at any location during an EQ mainly depends on three parameters; EQ magnitude, epicenter distance and local soil conditions. Among these three parameters, local soil condition has a higher influence on the surface motion characteristics (Apostolidis et al. 2006; Anbazhagan et al. 2011; Mohamed et al. 2013;

Kumar and Baro 2016; Mondal and Kumar 2016; Kumar et al. 2016, 2017a, b; Banerjee and Kumar 2017a, b; Kumar and Mondal 2017). The soil deposits can modify the input ground vibration by amplifying it at certain frequencies while deamplifying at other frequencies (Walling et al. 2009; Kumar et al. 2015). This phenomenon is known as local site effect and is a major factor responsible for the surface level of ground shaking witness during an EQ (Mirzaoglu and Dykmen 2003). Local site effect causes varying amplification in the ground motion resulting in non-uniform EQ induced damage patterns. The effects of local soil were evidenced during the 2001 Bhuj EQ. Amplification of ground motions by the soil layers caused severe damage in areas far from the epicenter (Mahajan and Kumar 2004). Ahmedabad, Bhuj, Rajkot, Anjar and Gandhidham regions spreading over 350 km away from the epicenter were amongst the severely affected areas (Verma et al. 2014). This EQ caused severe damages to the dams at Fategadh, Kaswati, Suvi, and Tapar, built on alluvial soil (Krinitzsky and Hynes 2002). Another example is the 2011 Sikkim EQ (Mw = 6.9), where the epicenter was located north-west of Chungthang towards the Indo-Nepal border in Sikkim. Even though the size of the EQ was moderate, it caused considerable damage to the buildings in the northern parts of Bihar, eastern Nepal, southern Bhutan and parts of Tibet (Mahajan et al. 2012), located several hundreds of kilometers away from the epicentre. Instances reported above from the Indian subcontinent are clear indications of the fact that local site is responsible for a majority of the damages not only in the epicentral region but at farther distances as well, during a moderate to major EQ event. Hence, effective estimation of the influence of local site, upon bedrock motion, is an

[1] Department of Civil Engineering, Indian Institute of Technology Guwahati, Assam, India. E-mail: abhiak@iitg.ernet.in

important factor in understanding the surface ground motion scenario and the possible extent of induced damages during an EQ.

SC has been one of the key issues in EQ engineering. Most of the classification systems proposed till date [such as, National Earthquake Hazards Reduction Program (NEHRP BSSC 2003); Eurocode 8; International Building Code (IBC 2009)] use top 30 m based average N-SPT (N_{30}) or 30 m average shear wave velocity (V_{s30}) or Cu values for the determination of SC. V_{s30} is popular because it is comparatively a simple parameter and the data acquisition is faster (Martin and Diehl 2004). However, several researchers including Stephenson (2007), Park and Hashash (2004) have raised doubts regarding the effectiveness of V_{s30} to predict site amplifications. Lee and Trifunac (2010) demonstrated that V_{s30} should not solely be considered to represent the site amplification. Later, Luzi et al. (2011) proposed SC chart based on soil predominant frequency (f_{peak}) obtained from HVSR of EQ records, either as an alternative or as a complement to V_{s30}.

Strong motion recordings are widely used in several seismic zonation and seismic risk analyses. Development of ground motion prediction equation (GMPE) requires regional ground records. Number of researchers have attempted seismic hazard analyses of different cities in India. Most of these studies, however, provide the seismic hazard values at bedrock level in the absence of regional subsoil characteristics. It has to be mentioned here that the application of such studies to provide surface level seismic hazard values are very limited. In addition, quantification of induced effects cannot be attempted based on available bedrock level seismic hazard studies. A good quality accelerogram should include information regarding the station location, EQ sources, ground motion parameters and Sc. Accurate assessment of SC of strong motion station is required to determine the suitability of strong motion recordings for specific application. PESMOS (http://www.pesmos.in/) is one of the most significant sources of ground motion records in India. The recording stations do not have adequate subsoil information. Therefore, no accurate assessment of SC is available at present. In the present study, strong ground motion records from 90 seismic stations located in the

northwestern Himalayas and the adjoining region are used to develop HVSR curves to determine the SC of each of these recording stations.

2. Theoretical Background

To understand the subsoil characteristics, Nakamura (1989) proposed a methodology using horizontal to vertical ratio of Fourier spectrum of recorded ambient noises (called microtremors) produced from artificial sources. Nakamura (1989) technique was based on the assumption that only the horizontal component of ground motion record retains the soil amplification characteristics while the source and the propagation path characteristics are maintained in both vertical as well as horizontal components of ground motion. Thus, the Fourier ratio of horizontal to vertical components of ground motion (HVFR) record eliminates the source and propagation path effect and gives the site characteristics alone. Later, Yamazaki and Ansary (1997) analyzed HVFR of strong ground motion data from Japan Meteorological Agency and reported the stability of the method, regardless of the magnitude of EQ. In another work, Theodulidis and Bard (1995) compared the HVFR of strong ground motion calculated from Greece and Taiwan accelerograms with the theoretically estimated amplification transfer function and reported good similarities in terms of the f_{peak} values. Highlighting the challenges in obtaining HVFR curves in terms of obtaining clear and distinct peaks, to determine the f_{peak} values, horizontal to vertical spectral ratio (HVSR) was proposed by Zhao et al. (2006) considering 5% as system damping. With this specific advantage, HVSR has become popular in understanding the site characteristics. Zhao et al. (2006) developed an empirical classification scheme based on the f_{peak} values obtained from the HVSR using K-net strong motion records in Japan.

3. Study Area

The entire Himalayan arc is approximately 2500 km in length, extending from Kashmir in the

northwest to Arunachal Pradesh in the northeast. The seismicity of this region is due to the continued convergence of the Indian plate against the Eurasian plate (Srivastava et al. 2013; Anbazhagan et al. 2013). This convergence started approximately about 50 million years ago and at present the rate of collision between the two plates is 5 cm per year. This collision resulted in uneven stress accumulation and subsequent formation of a series of thrust sheets, at different segments (Mugnier et al. 2013), along the 2500 km Himalayan belt. The entire Himalayan belt, based on seismic activity, has been classified into three distinct segments namely; the Western, the Central and the Eastern segment. For the present work, the northwestern segment of the Himalayas located to the west of 1905 Kangra EQ, is considered for the determination of SC of the recording stations. Some of the major populated urban centers in India such as Dehradun, Haridwar, Roorkee, Amritsar, Delhi and many more are in close vicinity of the northwestern Himalaya. Tectonic features in the region includes the Main Central thrust (MCT), the Main Boundary thrust (MBT), the Karakoram fault, the Malari Fault, the Jhelum Balakot fault (JBF), the Jwala Mukhi thrust (JMT), the Drang thrust (DT), the lesser Himalayan Crystalline Nappes (LHCN), the Jammu thrust, the Vaikrita thrust, the Ramgarh thrust (RT) and the Himalayan frontal thrust (HFT). Among these, the MCT, the MBT and the HFT are considered to be the most tectonically active seismic sources in the region (Ni and Barazangi 1984). Some of the active faults between the HFT and the MBT had generated major EQs in the region (Philip et al. 2014). The most prominent EQs in the span of last 120 years in the western Himalayan zone include 1905 Kangra-Himachal Pradesh EQ ($M_s = 7.8$) (Ambraseys and Douglas 2004) and 2005 Muzzafarbad-Kashmir EQ ($M_w = 7.6$) (Avouac et al. 2006). Both these EQs had caused severe loss of life and infrastructure. The more recent 1999 Chamoli EQ and 1991 Uttarkashi EQ occurred on the MCT zone (Harbindu et al. 2014; Kayal 1996). The 1999 Chamoli EQ caused a huge landslide in Gopeshwar, situated less than 2 km northwest of Chamoli city (Sarkar et al. 2001). The region of Delhi is of strategic importance being the national capital. In addition to the western Himalayas, regional active

sources in the adjoining areas exist adjoining the national capital namely the Mahendragarh fault, the Delhi Haridwar fault, the Sohna fault, the Delhi Meerut fault and the Rajasthan boundary fault (Iyengar and Ghosh 2004).

4. HVSR Calculation

Fourier spectra of EQ record in general contains many spikes. Thus, smoothening of the Fourier spectra is essential for identifying a clear and distinct peak (Konno and Ohmachi 1998). Figure 1a shows the HVFR curve based on recorded ground motions at Champawat recording station during July 2010 EQ. It can be observed from Fig. 1a that the HVFR curve contains several spikes, with no distinct peak. This creates difficulty in computing the f_{peak} for the Champawat recording station. The number of spikes in the HVFR curve vary drastically from one EQ record to another, for the same recording station. Thus, the extent of smoothening varies for different
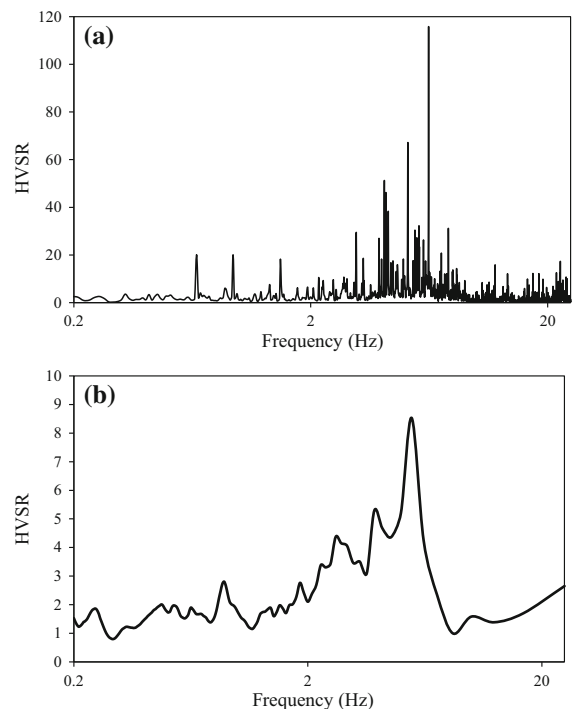

Figure 1
Comparison between horizontal to vertical ratio of Fourier Spectra (**a**) and response spectra (**b**) for Champawat station

records even at the same station to get clear peaks. The site response characteristics obtained from the HVFR curve thus vary with the extent of smoothening (Zhao et al. 2006). Theoretically, the Fourier amplitude spectra can be approximated by the relative velocity response spectra with a low value of damping ratio (Yamazaki and Ansary 1997).

Based on the work, Zhao et al. (2006) concluded that instead of considering the ratio of horizontal to vertical records in terms of Fourier spectra, if the ratio of spectral acceleration for 5% damping is considered, it will have significant effect on smoothening. The 5% damped acceleration spectra have a spectral shape which is similar to that of the Fourier spectra except that the sharp peaks of the Fourier spectra (see Fig. 1a) are not present in the response spectra (see Fig. 1b). In addition, the number of spikes will be reduced considerably, thus giving a clear peak. Moreover, the extent of smoothening will be uniform for all the records. Thus, HVSR will provide consistent results independent of ground motion records (Zhao et al. 2006). Compared to Fig. 1a, b has lesser spikes and thus the peaks are clearly visible. With this observation, further analyses in this work are done based on HVSR curves instead of HVFR curves. To determine the HVSR, the following procedure has been adopted;

- Considering 5% damping ratio value, calculate the response spectra for the three components (north–south, east–west and vertical) of ground motion records.
- Smoothen the response spectra of each of the three components using a Konno-Ohmachi (1998) window with a bandwidth parameter b of 20.
- Obtain the geometric mean of the two horizontal response spectra components (H) using the Eq. (1) below;

$$H = (H_{EW} \times H_{NS})^{0.5} \qquad (1)$$

- Calculate the ratio of H to V (H/V).

where, H_{EW} and H_{NS} are the pseudo response acceleration (PSA, 5% damped) of the horizontal east–west and north–south components, respectively, and V is the PSA of the corresponding vertical

component. Then, the HVSR at each station can be determined as;

$$(HVSR)_i = \frac{\sum_{i=1}^{Ni} \frac{H}{V}}{Ni} \qquad (2)$$

where Ni is the number of events recorded at station i. Further, $HVSR_i$ indicates the average HVSR value for a particular station i. The f_{peak} for a station is the frequency corresponding to the maximum value of $HVSR_i$ at that station. Based on f_{peak}, that particular recording station can be assigned a suitable SC.

The classification scheme adopted by PESMOS consists of three SCs namely; SC A, SC B and SC C following Borcherdt (1994). The general description about the ground for each SC is presented in column 2, Table 1 in accordance with Borcherdt (1994). It can be observed from Table 1 that PESMOS provides three SCs against V_{s30} varying between 200 and 1620 m/s. On the other hand, widely followed NEHRP (BSSC 2003) site classification scheme categorizes the local soil into five different SCs with a wide range of V_{s30} as shown in Table 2. Comparison of Tables 1 and 2 suggests that SC E as per NEHRP which is considered as potentially liquefiable soils is absent in Borcherdt (1994) classification scheme. For very hard rocks ($V_{s30} > 1620$ m/s), no SC is given as per Borcherdt (1994) which is classified as SC A as per NEHRP (BSSC 2003). The effectiveness of classifying site based on f_{peak} is already highlighted earlier. For further analysis in this work, the f_{peak} of different SCs given as per Borcherdt (1994) and NEHRP (BSSC 2003) should be calculated. For a single layer model over half space, the value of f_{peak} is correlated to the soil depth (H) and shear wave velocity (V_z) as per Eq. (3) below (Kramer 1996);

$$f_{peak} = \frac{V_z}{4H} \qquad (3)$$

Considering H as 30 m as overburden thickness, V_z will become V_{s30}. Based on the range of V_{s30} for various SCs, the range of f_{peak} is estimated in accordance with Eq. (3) as shown in column 4, Tables 1 and 2 considering 30 m as overburden thickness. Further, the values of f_{peak} for each of the 90 seismic station is determined based on ground motion records at each station during various EQs as discussed in the later section.

Table 1

Site classification scheme for strong motion recording stations as per PESMOS (modified after Mittal et al. 2012)

Site class 1	General description 2	Shear wave velocity (m/s) 3	Fundamental frequency (Hz) 4
A	Firm/hard rocks (Fresh and compact metamorphic e.g. gneiss, schist, migmatites, phyllites, quartzites, dolomites and igneous rocks e.g. granites, granodiorites, granitoids, basic volcanics)	700–1620	5.8–13.33
B	Soft to firm rocks (Sedimentary rocks e.g., sandstone, shale, limestone)	375–700	3.125–5.83
C	Soils (Alluvium, slope wash material, Aeolian)	200–375	1.667–3.12

Table 2

NEHRP site classification (BSSC 2003)

Site class 1	General description 2	Shear wave velocity (m/s) 3	Fundamental frequency (Hz) 4
A	Hard rock	> 1500	> 12.71
B	Rock	760–1500	6.35–12.70
C	Very dense soil and soft rock	360–760	3.05–6.35
D	Stiff soil	180–360	1.52–3.05
E	Soft soil	< 180	< 1.525

5. Data Bank

The seismicity of the western Himalayas and the adjoining Delhi area has been discussed earlier suggesting that both the regions have experienced significant damages during various EQs in the past. Thus, understanding the subsoil characteristics of both the regions is very important. For monitoring the ongoing seismicity in different segments of the active regions of India, 300 state of the art digital strong motion accelerographs were installed. These seismic recording stations are distributed in the northern and northeastern parts of India as well as in the Andaman and Nicobar Islands as a part of the "National Strong Motion Instrumentation Project" to monitor EQs (Kumar et al. 2012). Information regarding the instrumentation, processing of records and networking of the accelerographs was reported by Kumar et al. (2012). The strong motion records from the above seismic recording stations are available from PESMOS website (http://www.pesmos.in/) within the period of 2004 till present. In the present study, ground motion records from 90 seismic recording stations under PESMOS, are considered for the analyses. All these recording stations are located in

the parts of northwestern Himalayas as well as regions in and around Delhi as shown in Fig. 2. It can be seen in Fig. 2 that the recording stations are covering the states of Punjab, Himachal Pradesh, Haryana, Uttarakhand and Delhi. In addition, a uniform distribution of seismic recording stations in Uttarakhand and Himachal Pradesh regions can be seen from Fig. 2. On the other hand, a dense network of seismic stations can be seen for Delhi from Fig. 2. It has to be mentioned here that numbers given in Fig. 2 for various recording stations in each state are corresponding to Sl. No. given in Table 3. Further, states of Jammu and Kashmir and Uttar Pradesh have 1 and 3 recording stations which are presented in the combined map of states (see E in Fig. 2).

Seismic activity of these recording stations can be understood from the fact that 1905 Kangra EQ (M-7.8), occurred in Himachal Pradesh while events such as 1991 Uttarkashi EQ (M-6.8) and 1999 Chamoli EQ (M-6.5) occurred in the Uttarakhand region. Similarly, Punjab is also seismically active having witnessed events such as 1952 Kapurthala EQ (M-5.2). On the other hand, some of the past EQs that occurred in Delhi including 1720 EQ (M-6.5), 1830 EQ, 1956 EQ (M-6.0), etc. highlight the alarming seismic activity of
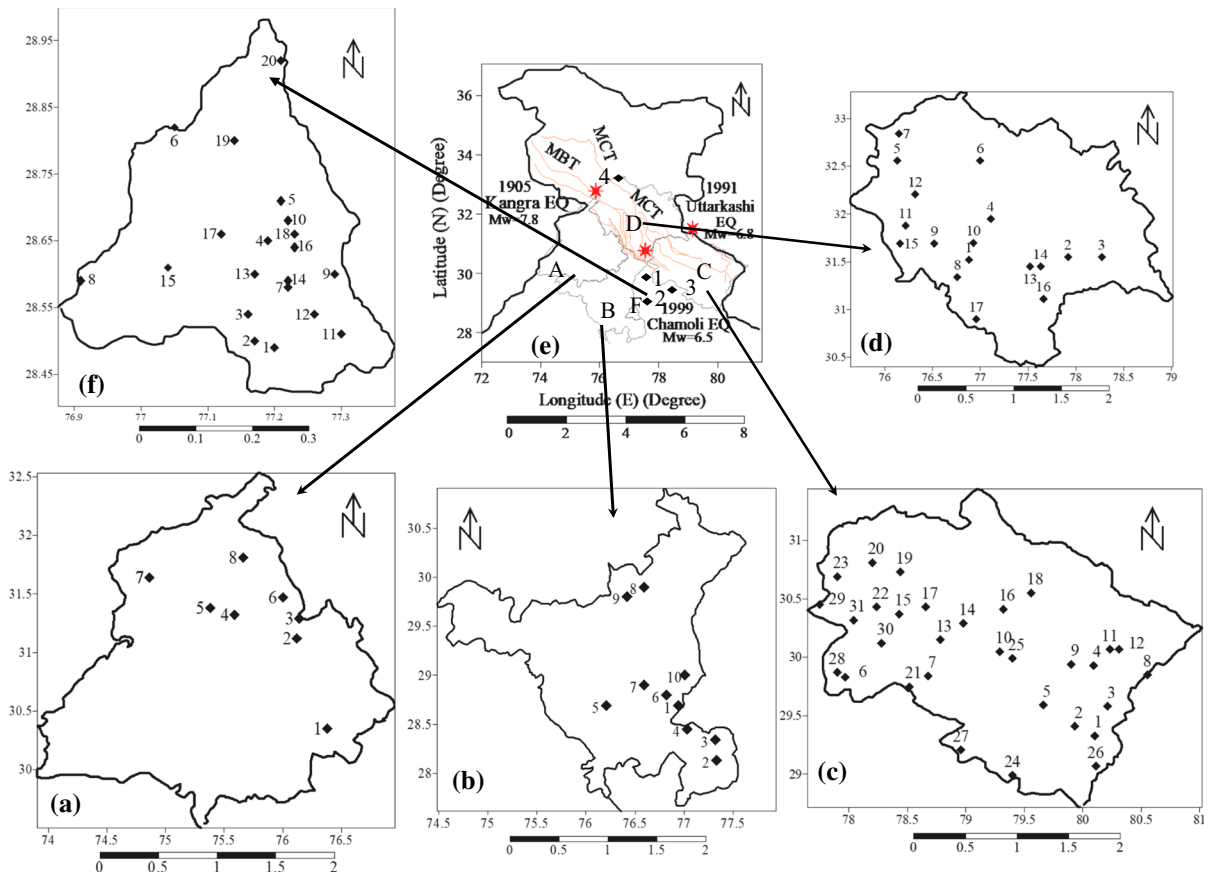
Figure 2
Locations of PESMOS recording stations used in the present study (Note: A-Punjab; B-Haryana; C-Uttarakhand; D-Himachal Pradesh; E presents recording stations 1, 2, 3 from Uttar Pradesh and 4 from Jammu and Kashmir; F-Delhi)

Delhi. Table 3 lists all the 90 recording stations used in the present work. It has to be highlighted here that a number of stations having the same name but different coordinates are also available in PESMOS. To handle larger database, recording stations with same name are nomenclature in this work as Rohtak 1 and Rohtak 2 shown in Table 3, column 2. SC for each recording station as given by PESMOS is listed in Table 3, column 3. It can be observed from Table 3, column 3 that a majority of the recording stations are assigned SC C while a significant number of recording stations also belong to SC A. Very limited number of recording stations belong to SC B. Table 3, column 6 and 7 give the standard deviation in f_{peak} and A_{peak}, respectively. The value of standard deviation of f_{peak} varies from 0.02 to 2.8. The low value of standard deviation

indicates the stability of f_{peak} of various EQs for a particular recording station. The value of standard deviation in case of A_{peak} is in the range of 0.26–3.75 as can be observed from Table 3, column 9.

To examine the site characteristics, 300 ground motion records generated during 52 EQs and recorded at above 90 recording stations are considered in the present work. The epicenter location of all the 52 EQ events used in the present study is presented in Table 4. It can be observed from Table 4, column 5 that magnitude (M_w) of EQ considered in this work varies from 3.5 to 6.8. In addition, ground motion records for moderate events, such as the Hindu Kush EQs of 01st January 2009 ($M = 6.4$), and of 17th September 2010 ($M = 6.5$), are included in the dataset.

Table 3

Detail of strong motion recording station

SI no. 1	Station 2	a 3	f_{peak} (Hz) 4	A_{peak} 5	b 6	c 7	d 8	e 9	SI no. 1	Station 2	a 3	f_{peak} (Hz) 4	A_{peak} 5	b 6	c 7	d 8	e 9
Delhi									*Uttarakhand*								
1	Rohtak 1	A	5.00	3.91	B	C	0.90	2.10	1	Champawat	A	5.55	6.50	B	C	0.78	1.85
2	Rohtak 2	A	5.60	3.50	B	C	0.88	2.10	2	Patti	A	3.85	7.80	B	C	0.66	2.5
3	JNU	A	12.5	2.56	A	B	0.62	1.52	3	Pithoragarh 1	A	4.54	3.10	B	C	0.58	2.14
4	Karol Bagh Delhi	A	10.00	4.52	A	B	2.80	2.46	4	Pithoragarh 2	A	5.55	6.90	B	C	0.87	3.33
5	DHB 1	A	7.14	3.77	A	B	2.80	2.46	5	Almora	A	2.94	4.20	C	D	0.87	0.93
6	DHB 2	A	4.17	9.39	B	C	1.50	2.50	6	Bageshwar	A	1.52	5.20	C	E	0.18	1.25
7	DHB 6	C	1.07	5.16	–	E	0.49	2.00	7	Lansdown	A	6.18	4.50	A	C	0.53	2.9
8	DHB 7	C	1.04	2.32	–	E	0.74	1.30	8	Dharchula	A	2.78	5.60	C	D	0.68	1.5
9	DHB 8	C	4.54	4.26	B	C	–	–	9	Kapkot	A	3.33	9.30	B	C	0.68	3.75
10	IMD	A	6.25	2.96	A	C	–	–	10	Garsain	A	2.27	4.50	C	D	0.36	2.08
11	NTPC	C	2.77	5.36	C	D	0.48	1.58	11	Munsyari 1	A	2.38	3.40	C	D	0.78	3
12	Kalkaji Delhi	C	4.17	4.60	B	C	0.23	0.75	12	Munsyari 2	A	1.60	3.50	–	D	0.47	2.15
13	Dhaula Kaun Delhi	C	3.84	3.20	B	C	0.41	1.30	13	Pauri	A	3.12	3.20	B	C	0.85	2.55
14	Delhi	C	1.08	6.78	–	E	0.37	2.50	14	Rudraprayag	A	1.47	5.90	–	E	0.07	2.12
15	NSIT	C	2.27	3.88	C	D	0.36	1.85	15	Tehri	A	1.5	5.50	–	E	0.48	0.55
16	Jakir hussain	C	3.57	7.06	B	C	0.52	1.45	16	Chamoli	A	1.51	7.50	–	E	0.08	3.51
17	Raja Garden Delhi	C	3.12	3.68	B	C	1.36	1.98	17	Ghansali	A	4.54	5.50	B	C	0.71	1.3
18	Iderprastha Univ	C	2.63	7.67	C	D	1.25	2.50	18	Joshimath	A	0.74	3.10	–	E	0.05	1.60
19	Alipur	C	2.50	6.67	C	D	0.29	2.30	19	Uttarkashi	A	2.17	4.40	C	D	0.87	1.80
20	Khatima	C	2.00	8.05	C	D	–	–	20	Barkot	A	3.33	5.50	B	C	0.47	2.03
Himachal Pradesh									21	Kotdwar	B	0.64	3.60	–	E	0.05	1.58
1	Sunder Nagar	A	5.00	3.78	B	C	1.20	0.68	22	Dhanaulti	B	1.85	7.10	C	D	0.5	1.60
2	Nathpa 1	A	4.54	4.36	B	C	0.36	1.80	23	Chakrata	B	1.92	4.50	C	D	1.41	0.49
3	Nathpa 2	A	4.54	4.36	B	C	0.25	2.30	24	USN	C	2.78	7.8	C	D	0.14	1.53
4	Kullu	A	3.12	3	B	C	1.10	1.80	25	USN 2	C	2.17	10	C	D	0.69	2.5
5	Chamba	A	1.92	2.94	C	D	0.14	1.50	26	Tanakpur	C	5.00	6.30	B	B	–	–
6	Keylang	A	16.67	2.20	–	A	2.00	1.05	27	Kashipur	C	3.12	9.90	B	C	–	–
7	Tissa	A	10.00	3.37	A	B	1.60	1.90	28	Roorkee	C	1.52	5.30	–	D	0.09	0.26
8	Bilaspur	B	0.26	2.9	–	E	0.02	0.69	29	Vikas Nagar	C	2.27	8.30	C	D	0.29	2.52
9	Hamirpur	B	3.33	6.6	B	C	0.39	2.30	30	Rishikesh	C	3.33	6.40	B	C	–	–
10	Mandi	B	2.50	5.11	C	D	0.95	1.69	31	Dehradun	C	3.12	7.40	B	C	–	–
11	Dehra	B	10.00	5.40	A	B	1.69	2.30	*Jammu and Kashmir*								
12	Dharmashala	B	2.78	4.17	C	D	0.73	2.15	4	J and K	A	2.78	5.8	C	D	0.96	1.69
14	Rampur 1	A	2.63	5.57	C	D	0.47	2.81	*Haryana*								
13	Rampur 2	C	2.50	4.03	C	D	0.54	1.36	1	DHB 3	C	2.94	3.90	C	D	0.29	2.18
15	HM Punjab 1	C	flat	flat	–	–	–	–	2	DHB 4	C	2.94	3.40	C	D	0.69	2.36
16	Jubbal	A	5.56	4.48	B	C	0.66	1.47	3	DHB 5	C	0.78	3.60	–	E	0.03	1.69
17	Kasauli	B	2.08	10.3	C	D	0.05	1.69	4	Gurgoan Delhi	C	0.98	6.80	–	E	0.05	1.56
Punjab									5	Rohtak 3	C	1.92	3.70	C	D	1.61	0.37
1	Patiala	C	1.00	5.95	–	E	0.09	1.69	6	Rohthak 4	C	5.00	4.20	B	C	0.29	1.36
2	Nawan Shahar	C	1.11	8.57	–	E	0.27	2.66	7	Rohtak 5	C	2.08	2.90	C	D	0.36	1.63
3	Garsain	C	0.83	8.7	–	E	0.06	2.14	8	Jhajjar	C	2.20	4.60	C	D	0.37	2.10
4	Jalandhar	C	1.67	7.4	C	D	0.97	2.55	9	Kaithal	C	1.11	5.70	–	E	0.03	1.69
5	Kapurthala	C	1.8	2.51	C	D	0.09	0.69	10	Sonipat	C	2.78	4.50	C	D	0.45	2.14
6	UNA	C	1.78	5.8	C	D	0.82	2.61	*Uttar Pradesh*								
7	Amritsar	C	1.04	5.99	–	E	0.58	2.13	1	Sangur	C	1.85	2.90	C	C	0.58	1.35
8	HM Punjab 2	C	1.20	9.5	–	E	0.29	2.69	2	Gautombudh	C	2.08	5.20	C	D	0.58	1.85
									3	Baraut	C	1.39	4.30	–	E	0.58	1.69

DHB Delhi Haryana Border, *USN* Udham Singh Nagar

[a]SC as given in PESMOS

[b]SC as per PESMOS based on f_{peak}

[c]SC as per NEHRP

[d]Standard Deviation in f_{peak}

[e]Standard Deviation in A_{peak}

Table 4

Details of earthquakes considered in this work

Sl. no.	Date	Latitude (Degree) (N)	Longitude (Degree) (E)	Magnitude	Focal depth (km)	Sl. no.	Date	Latitude (Degree) (N)	Longitude (Degree) (E)	Magnitude	Focal depth (km)
1	14-12-2005	30.90	79.30	5.20	25.70	27	11-01-2010	29.70	80	3.9	15
2	10-12-2006	31.50	76.70	3.50	33	28	22-02-2010	30	80.1	4.7	2
3	22-07-2007	31.20	78.20	5	33	29	26-02-2010	28.50	86.7	5.4	28
4	04-10-2007	32.50	76	3.80	10	30	14-03-2010	31.70	76.1	4.6	29
5	13-03-2008	26.60	91.80	4	33	31	01-05-2010	29.90	80.1	4.6	10
6	29-05-2008	26.60	91.80	4.20	33	32	03-05-2010	30.40	78.4	3.5	8
7	19-08-2008	30.10	80.10	4.30	15	33	28-05-2010	31.20	77.9	4.8	43
8	04-09-2008	30.10	80.40	5.10	10	34	31-05-2010	30	79.8	3.6	10
9	06-09-2008	36.70	70.60	5.80	160	35	06-07-2010	29.80	80.4	5.1	10
10	21-10-2008	31.50	77.30	4.50	10	36	10-07-2010	29.90	79.6	4.1	10
11	25-12-2008	27.20	87.90	4.40	33	37	26-07-2010	26.50	91.3	4.1	31
12	03-01-2009	36.50	70.80	6.40	188	38	17-09-2010	36.50	70.8	6.5	167
13	09-01-2009	31.70	78.30	3.80	16	39	21-03-2011	36.50	70.9	5.7	166
14	31-01-2009	32.50	75.90	3.70	10	40	04-04-2011	29.60	80.8	5.7	10
15	25-02-2009	30.60	79.30	3.70	10	41	04-05-2011	30.20	80.4	5	10
16	25-04-2009	26.40	91.70	4	10	42	20-06-2011	30.50	79.4	4.6	12
17	15-05-2009	30.50	79.30	4.10	15	43	22-09-2011	27.60	88.4	3.9	30
18	17-07-2009	32.30	76	3.70	39.30	44	16-01-2012	29.70	78.9	3.6	10
19	19-08-2009	26.60	92.50	4.90	20	45	09-02-2012	30.90	78.2	5	10
20	27-08-2009	30	80	3.90	14	46	26-02-2012	29.60	80.8	4.3	10
21	21-09-2009	30.90	79.10	4.70	13	47	11-05-2012	26.60	93	5.4	20
22	03-10-2009	30	79.90	4.30	15	48	10-07-2012	26.50	93.2	4.5	56
23	22-10-2009	36.50	71	6.30	168	49	12-07-2012	36.50	70.9	6.3	70
24	29-10-2009	26.60	90	4.20	10	50	28-07-2012	29.7	80.7	4.5	10
25	06-12-2009	35.80	77.30	5.30	60	51	23-08-2012	28.4	82.7	5	10
26	31-12-2009	27.30	91.40	5.50	7	52	17-06-2014	32.2	76.1	4.1	10

6. Analysis and Results

Based on the above selected ground motions, HVSR curves are estimated for each of the 90 recording stations following earlier discussed procedure. In addition, the effect of magnitude and hypocentral distance, as a part of EQ records on SC and nature of HVSR curves, is also assessed in the following subsections.

6.1. Effect of Hypocentral Distance and Magnitude

Based on the three components of ground motions recorded at each station during an EQ, HVSR curve is estimated in accordance with Eqs. (1) and (2) as discussed earlier. To check the effect of EQ characteristics (magnitude and hypocenter distance) on the HVSR parameters such as A_{peak} and f_{peak} values, plots of HVSR curves during EQs of different magnitudes and hypocenter distances at each recording station are studied. Figure 3a shows typical HVSR curves
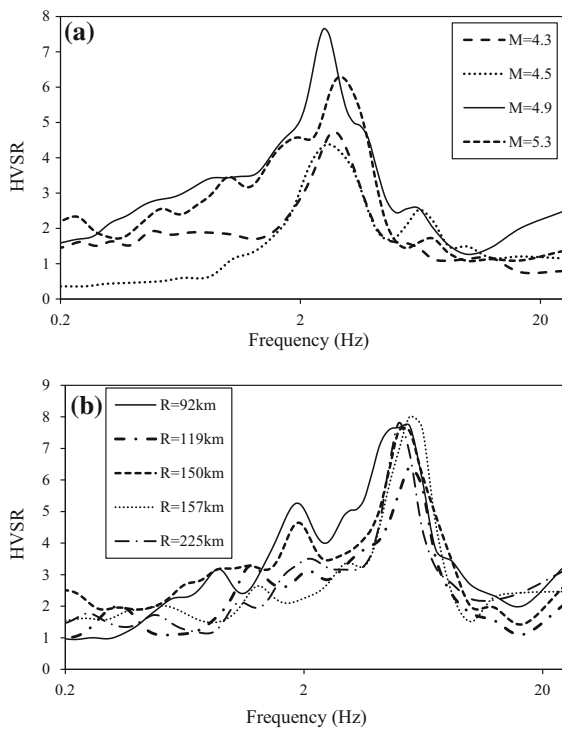
obtained during EQ's of different magnitude recorded at Rampur 2 station. Four different HVSR curves are obtained for four different magnitudes as shown in Fig. 3a. It can be observed from Fig. 3a that the shape of the HVSR curve and the f_{peak} value for this Rampur 2 station is remarkably similar even for different magnitude EQ. The amplification value from HVSR curves shows a wide variation, not following a particular trend. Since in the present work, only SC is attempted, the value of f_{peak} is observed carefully and not the A_{peak} value. Further, to understand the effect of hypocentral distance upon HVSR curve and f_{peak} value, the plot of HVSR curves obtained from EQs happened at different hypocentral distances (92–225 km) are plotted for Champawat station as shown in Fig. 3b. It can be observed from Fig. 3b that the shape of HVSR curve and the f_{peak} for this particular station are consistent and independent of hypocentral distance. Similar trends are also observed for other recording stations considered in the present work. Collectively, based on Fig. 3a, b, it can be concluded that the shape of HVSR curve and the f_{peak} value are independent of the EQ characteristics and solely demonstrate the SCs.

6.2. Average HVSR Curve for Recording Stations

Once the effects of EQ magnitude and hypocentral distance are examined, the average HVSR curves considering all ground motion records at each of the 90 recording stations are developed. Figure 4a–x presents typical average HVSR curve for 24 typical recording stations. It can be observed from Fig. 4a–x that each of the graph shows a distinct value of f_{peak}. To understand further, a detailed comparison in terms of HVSR curve for different SCs is attempted. The average HVSR curves at the Karol Bagh, Delhi Haryana Border 1, IMD station and Rohtak 2 stations are assigned SC A as per PESMOS. All these recording stations are located in the Delhi region. The values of f_{peak} estimated based on average HVSR curve are found to be 10, 7.14, 6.25 and 5.6 Hz for the Karol Bagh, Delhi Haryana Border 1 and IMD stations, respectively, as shown in Fig. 4a–c. It can be observed from Fig. 4a–c that recording stations at Karol Bagh exhibits clear distinct peaks, while IMD and Delhi Haryana Border one recording stations
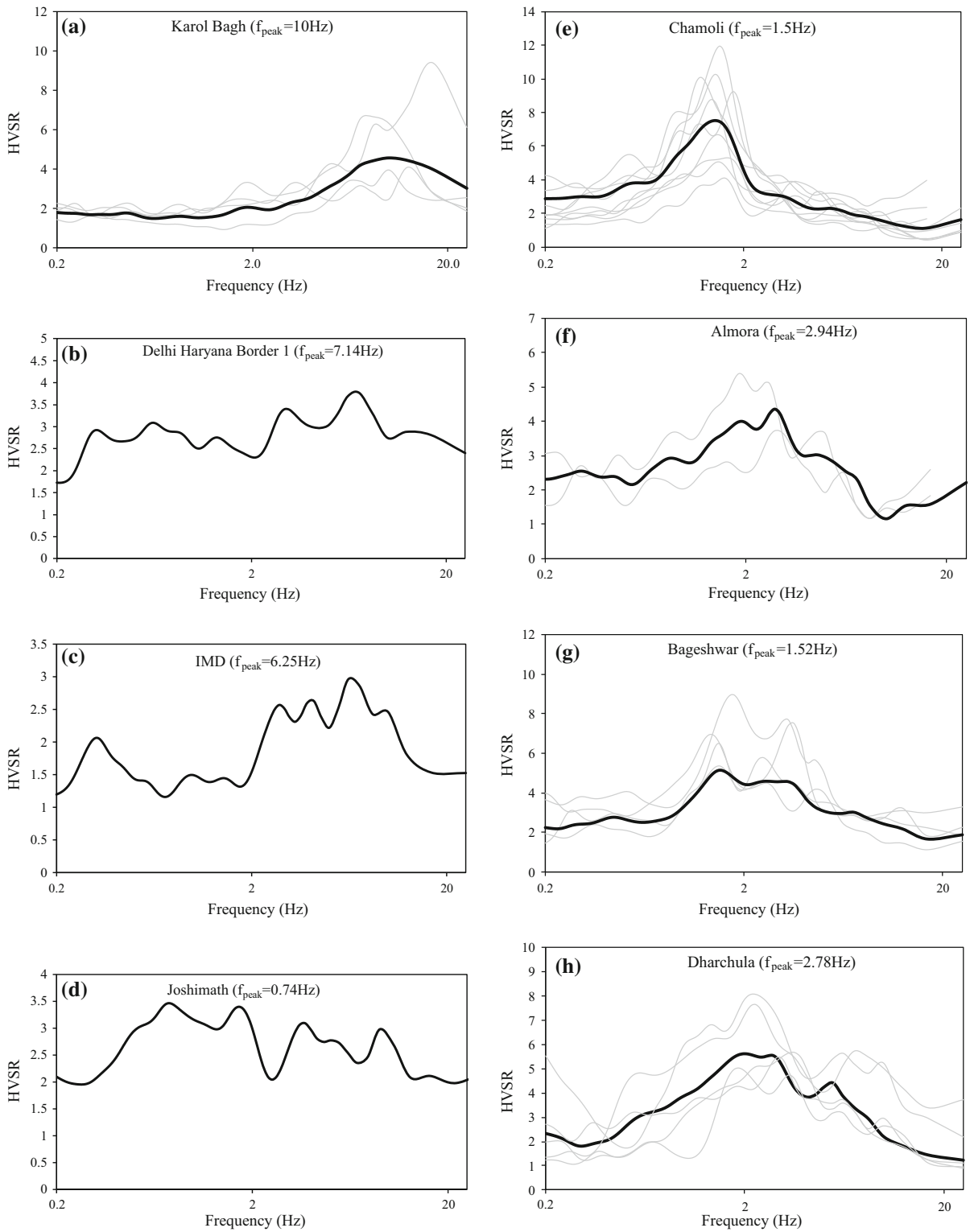
Figure 3
a Variation of HVSR curves with magnitude (Rampur 2 station); **b** Variation of HVSR curves with hypocentral distance (Champawat station)

Figure 4
a–x Typical HVSR curves for various recording stations

Figure 4
continued

(q) Delhi Haryana Border 8 (f$_{peak}$=4.54Hz)

(u) Kashipur (f$_{peak}$=3.12Hz)

(r) Rohthak 4 (f$_{peak}$=5Hz)

(v) Rishikesh (f$_{peak}$=3.33Hz)

(s) Khatima (f$_{peak}$=2Hz)

(w) Dehradun (f$_{peak}$=3.12Hz)

(t) Udham Singh Nagar (f$_{peak}$=2.78Hz)

(x) Tanakpur (f$_{peak}$=5Hz)
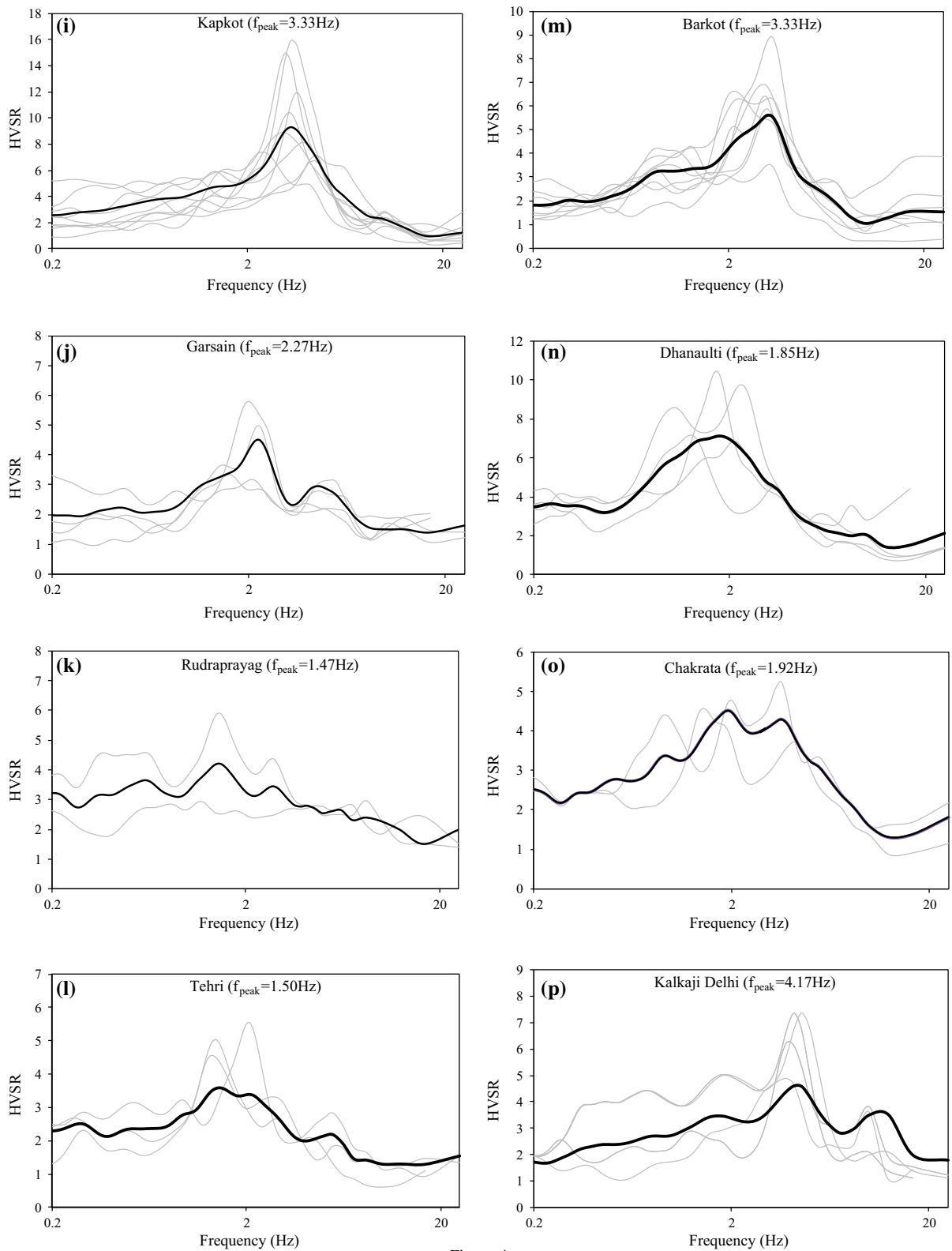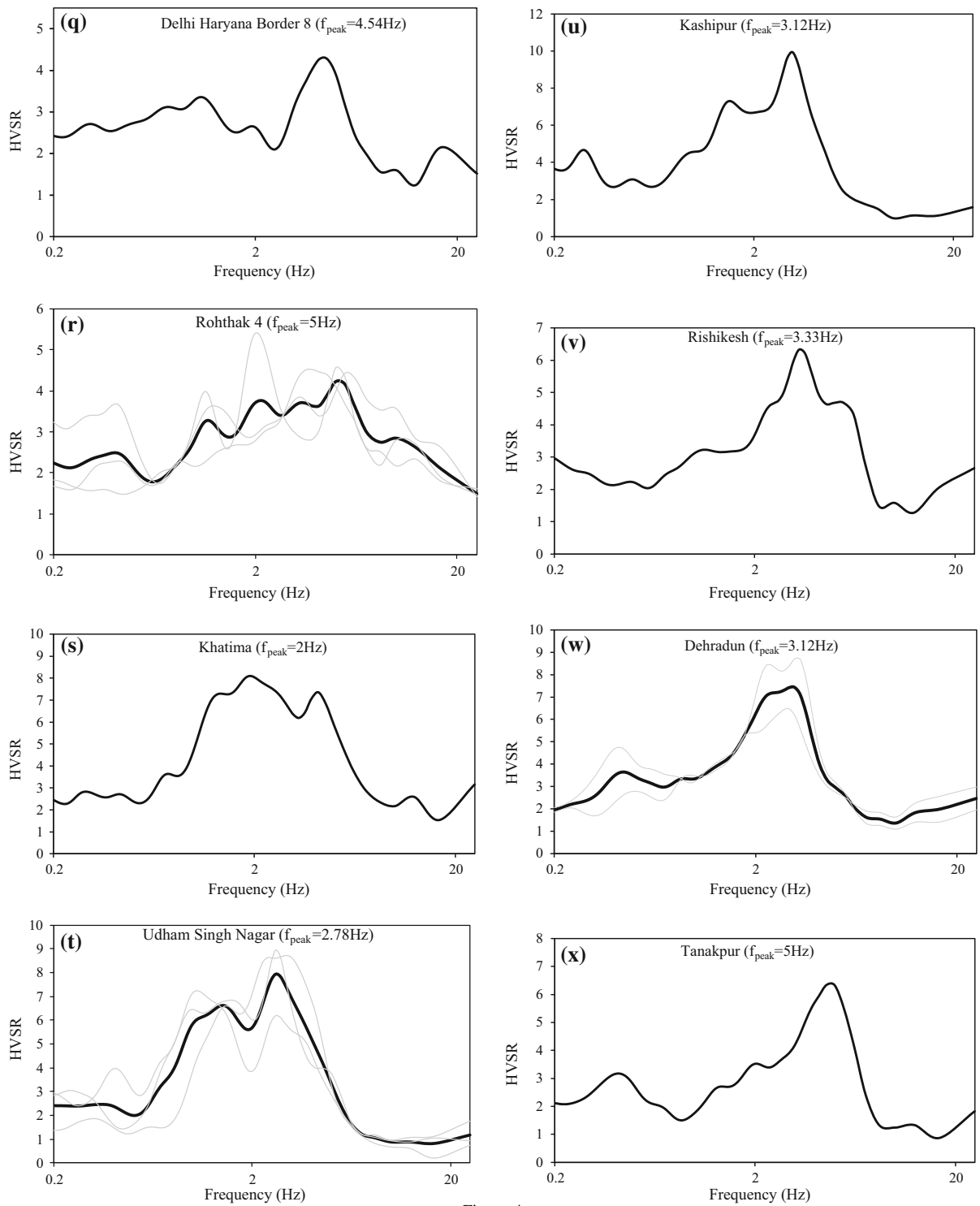
Figure 4
continued
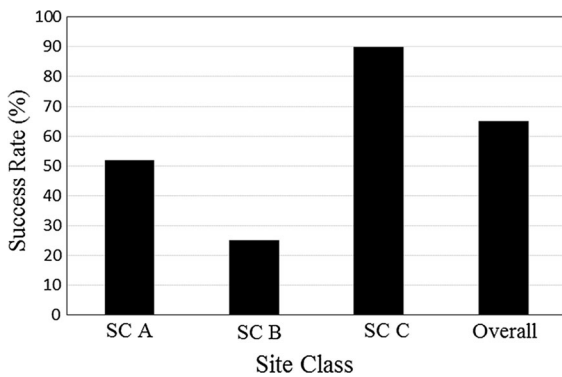
Figure 5
Success rate of the PESMOS classification scheme

Figure 6
Average HVSR for SC B, C, D, and E from the present work

Table 5

Number of stations in each NEHRP SC

NEHRP site class	Number of stations
SC A	1
SC B	6
SC C	29
SC D	33
SC E	20

show several peaks. Determination of f_{peak} value for Delhi region was also attempted by Sharma et al. (2004) based on microtremor studies. Comparison of f_{peak} values for all the above four stations obtained in the present work are found consistent with the results obtained by Sharma et al. (2004). The observed A_{peak} for Karol Bagh recording station (A_{peak} = 4.52) and Delhi Haryana Border 1 station (A_{peak} = 3.77) are slightly higher than the value reported by Sharma et al. (2004). It has to be highlighted here that the objective of present work is to classify the site based on f_{peak} value. Determination of A_{peak} is beyond the scope of the present work. Comparison in terms of f_{peak} value done above is also attempted for other stations where similar data from the previous literature are available. The average HVSR curves at Joshimath and Chamoli recording stations are shown in Fig. 4d, e suggesting f_{peak} values equal to 0.74 and 1.5 Hz, respectively. These values of f_{peak} match well with the passive survey results of Mahajan et al. (2011) suggesting SC C as per Table 1 for both these recording stations. However, the f_{peak} value for the above two recording stations do not match with the PESMOS SC A provisions. Further, the value of f_{peak}

for the recording stations at Almora (f_{peak} = 2.94 Hz), Bageshwar (f_{peak} = 1.52 Hz), Dharchula (f_{peak} = 2.78 Hz), Kapkot (f_{peak} = 3.33 Hz), Garsain (f_{peak} = 2.27 Hz), Rudra-prayag (f_{peak} = 1.47 Hz), Tehri (f_{peak} = 1.50 Hz) and Barkot (f_{peak} = 3.33 Hz) (as shown in Fig. 4f–m) are not matching with SC A assigned by PESMOS. However, these values of f_{peak} for the above recording stations are consistent with Sharma et al. (2014).

For recording stations at Dhanaulti and Chakrata (see Fig. 4n–o) the values of f_{peak} are observed to be less than 2 Hz. The average HVSR curve at Dhanaulti recording station exhibits a clear and distinct peak as shown in Fig. 4n. Mundepi (2013) reported the value of f_{peak} of 2.10 Hz for Dhanualti region. Based on the present work, the value of f_{peak} is found as 1.85 Hz for Dhanualti recording station which is closely matching with the findings of Mundepi (2013). Hence, Dhanaulti recording station has to be reclassified as SC C in the present work. For recording stations Kalkaji Delhi, Delhi Haryana Border 8 and Rohtak 4, the values of f_{peak} observed in the present work are greater than 4 Hz (see Fig. 4p–r). Mittal et al. (2013) reported the value of f_{peak} in the range of 4.3–4.6 Hz for the Kalkaji region in Delhi using standard spectral ratio method. Based on average HVSR curve, the value of f_{peak} of 4.17 Hz obtained from the present work for the Kalkaji Delhi recording station is matching closely with Mittal et al. (2013). Hence, the Kalkaji Delhi station has to be reclassified as SC A based on this work. Pandey et al. (2016) computed the V_z profiles for 12 recording
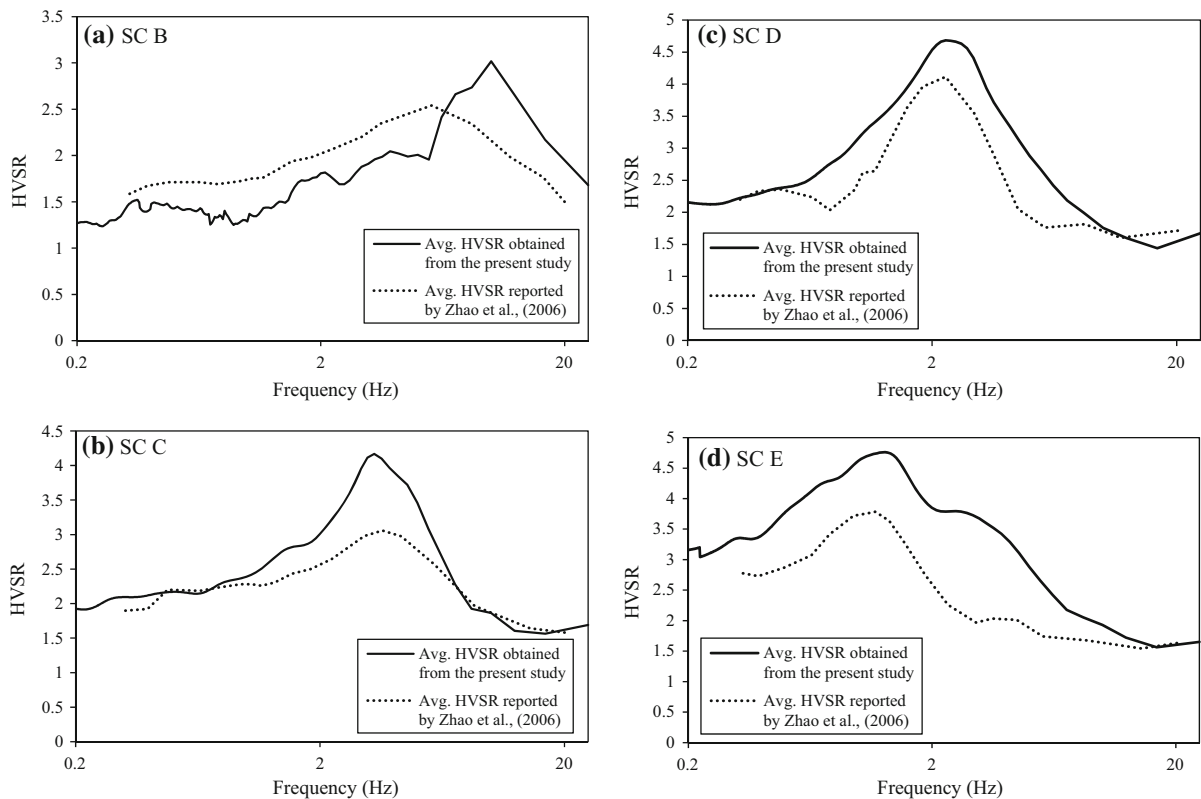
Figure 7

a–d Comparing the average HVSR ratios of northwestern Himalayan region obtained in this study and the average HVSR determined by Zhao et al. (2006) for Japanese strong motion sites for SC B, SC C, SC D and SC E respectively

stations situated in the Tarai region of Uttarakhand using MASW tests. Based on V_{s30} values, Pandey et al. (2016) classified the recording stations at Khatima, Udham Singh Nagar, Kashipur, Rishikesh and Dehradun (see Fig. 4s–w) as SC C as per PESMOS classification scheme. Based on f_{peak}, SC obtained in the present work for above recording stations are matching with the SC provision by PESMOS as well as Pandey et al. (2016). For Tanakpur recording station the value of f_{peak} from present work is found as 5 Hz (see Fig. 4x) which is closely matching with SC B assigned for this recording station by Pandey et al. (2016). Originally Tanakpur was assigned SC C as per PESMOS. In recent work, Harinarayan and Kumar (2017) attempted SC for all the 12 recording stations considered by Pandey et al. (2016) for based on model HVSR and using Eq. 3 and found matching.

Based on the above findings, it can be concluded that the values of f_{peak} obtained in the present work are matching with the existing literature. This clearly indicates that in the absence of field investigation data, HVSR curves based on ground motion records provide a better understanding about subsoil characteristics. Based on the average HVSR curve, the value of f_{peak} is estimated for all the 90 recording stations as listed in Table 3, column 4.

6.3. Determination of Revised SC for the Recording Station

The value of f_{peak}, for each recording station has been compared with the range of f_{peak} given for each SC as per NEHRP scheme as given in Table 2, column 4. Success rate is defined as the percentage of total number of recording stations where the SC based on

f_{peak} value and the one given as per PESMOS are matching. Considering all the 90 recording stations, the success rate for various SC are compared in Fig. 5. It can be seen that the success rate was found highest for SC C and lowest for SC B as shown in Fig. 5. Since SC D is absent in PESMOS description, no success rate is present for SC D. It has to be highlighted here that for certain recording stations, f_{peak} is lesser than 1.67 Hz and thus in accordance with Table 1, no SC could be assigned to such stations. Collectively from Fig. 5, it can be observed that for SC other than B the success rate is lower. This suggests that the SC obtained from average HVSR curve is varying for the majority of the recording stations from the SC given as per PESMOS. In other words, the SC given by PESMOS and the SC obtained from the ground motion records are not consistent. For SC A, 18 out of 38 stations satisfy the SC provisions by PESMOS indicating a success rate of 52%. The success rate of recording stations assigned SC B site is the lowest with a value of 25%. Only 2 out of 8 stations satisfy the SC provisions by PESMOS. For recording stations located in SC C as per PESMOS the success rate is the highest of 90% as shown in Fig. 5. A total of 38 out of 42 recording stations satisfy the SC provisions of PESMOS. Based on the success rate collectively, it can be said that more than 65% data shows similarity of SC obtained from the present work with the SC given by PESMOS. Above analysis suggests that SC as per Borcherdt (1994) using f_{peak} value and the one given by PESMOS are not matching for the significant number of recording stations. Based on this observation, updated SC for all the recording stations following Borcherdt (1994) classification scheme is also proposed as listed in Table 3, column 6. Comparison between original SC (Table 3, column 3) and revised SC (Table 3, column 6) following Borcherdt (1994) scheme shows that a majority of the recording stations yield same SC from both classification schemes. However, for certain locations (Rohtak 1, Rohtak 2, Champawat, Pithoragarh, etc.), a change in SC is observed.

6.4. NEHRP Based SC Determination of the Recording Stations

The site classification scheme adopted by PESMOS has limited SC in comparison with the worldwide followed NEHRP classification scheme. The f_{peak} values estimated earlier are used further to classify each recording station following NEHRP classification scheme in coherence with Table 2 as shown in Table 3, column 7. By comparing Tables 1 and 2, it can be observed that PESMOS has only three SCs while NEHRP has five SCs for almost similar range of V_{S30} values, providing a more precise classification of a site. As per NEHRP the SCs are varying from A to E. As indicated earlier, SC E represents potentially liquefiable site. SC given by PESMOS does not highlight any recording station located on potentially liquefied site as suggested by NEHRP classification scheme.

Summary of NEHRP based SC for all the recoding stations is presented in Table 5. It can be observed from Table 5 that there is only a single station (Keylang) belonging to NEHRP based SC A. However, for SC B, C, D and E a total of 6, 29, 33 and 20 recording stations are found based on the present work. HM Punjab 1 is not assigned any SC since distinct peak was absent. Considering the average HVSR curves obtained from similar SC, overall average HVSR curve is developed for all the SCs B, C, D and E. Figure 6 presents the average HVSR for SC B, C, D and E with f_{peak} values of about 10, 3.125, 2.5 and 1.28 Hz, respectively. SC B indicates stiffer medium followed by SC C, D and E. For this reason, the f_{peak} value of SC B shown in Fig. 6 is highest followed by SC C, D and E.

7. Validation

To further validate the findings from the present work, the average of HVSR curves presented in Fig. 7a–d are compared with the average HVSR curves found by Zhao et al. (2006) as shown in Fig. 7a–d. Zhao et al. (2006) classification scheme had 4 SCs; SC 1, SC 2, SC 3 and SC 4. The SC 1 is approximately corresponding to NEHRP SC A and SC B. The SCs 2, 3 and 4 is approximately corresponding to NEHRP SCs C, D, and E. It can be observed from Fig. 7a–d that the shape as well as f_{peak} of HVSR curve for each SC obtained in the present work and that by Zhao et al. (2006) are matching very well for SC C, D and E. However, that

f_{peak} value for SC B obtained in the present study is higher side compared to the f_{peak} value as per Zhao et al. (2006). This may be due to the fact that present work groups soils having V_{s30} in the range of 760–1500 m/s as SC B, while Zhao et al. (2006) grouped soils having V_{s30} greater than 600 m/s as SC 1. This difference in the lower range of V_{s30} values between the present work and Zhao et al. (2006), might be an attribute for getting different values of f_{peak} as observed in Fig. 7a. One important observation to be highlighted here is that the comparison of HVSR curves shown in Fig. 7a–d are done only in terms of f_{peak} and the shape. However, different values of A_{peak} can be observed between the two HVSR curves as shown in Fig. 7a–d. This difference in A_{peak} value might be due to the fact that in present study more than 50% of the ground motion is corresponding to EQs having magnitude less than 4.5 magnitude. However, curves proposed by Zhao et al. (2006) used ground motion of EQ having magnitude greater than 5. Thus, in comparison to the present work, Zhao et al. (2006) used ground motions due to higher magnitude EQs. As per EPRI (1993), Ashford et al. (2000) and Kumar et al. (2016a), higher amplitude ground motions produce low amplification and vice versa. Thus, the difference in the HVSR curves in terms of A_{peak} values presented in Fig. 7a–d are the attributes of different magnitude ranges used in each study.

8. Nature of HVSR Curves

Limited knowledge about the subsoil characteristics is available for the recording stations at present as highlighted earlier. Thus, determination of f_{peak} from ground motion records to determine the SC of each recording station is attempted in the earlier sections. Rao et al. (2011) attempted to understand the nature of average HVSR curve at a recording station as a function of its subsoil characteristics. Based on the modal characteristics of average HVSR curves, 11 categories were proposed. These include; unimodal curves indicate that single and distinct peak in average HVSR bimodal curves having two distinct peaks and multiple model curves having multiple peaks. Unimodal curves denote undamped ground

motions with high impedance (Rao et al. 2011). Bimodal curves are characterized by alluvial deposits at a site while multimodal curves indicate alluvial soil underlain by rocks of volcanic origin with f_{peak} ranging from 3 to 6 Hz. Similar to the work by Rao et al. (2011), all the average HVSR curves obtained from the present work show four types of modal characteristics. Based on these characteristics, all the HVSR curves are categorized into four categories. Type I HVSR curves which are unimodal in nature with a clear f_{peak} and flat response either in the initial frequencies or in the later frequencies as shown in Fig. 8a. Type I HVSR curves are exhibited by 23% of all the recording stations. Type II are unimodal response curves with broader f_{peak} window as shown in Fig. 8b. In the present analyses, 19% of all the station exhibits Type II HVSR curves. Similarly, HVSR curve for Type III have two clear f_{peak} values with one f_{peak} having comparatively higher A_{peak} than the other as shown in Fig. 8c. In the present analyses, 23% of the recording stations exhibits Type III HVSR curve. Type 'IV' HVSR curves have more than two peaks with one of the peaks showing higher A_{peak} than the others as shown in Fig. 8d. Type IV HVSR curves are exhibited by 35% of the total recording stations. Multiple peaks in the HVSR curve occur due to multiple impedance contrast within a heterogeneous soil deposit (Guéguen et al. 2000). Paudyal et al. (2012), Rao et al. (2011) and Luzi et al. (2011) also reported multiple peaks based on HVFR of microtremor records. It has to be highlighted here that the above categorization of recording stations is done purely based on the nature of average HVSR curves
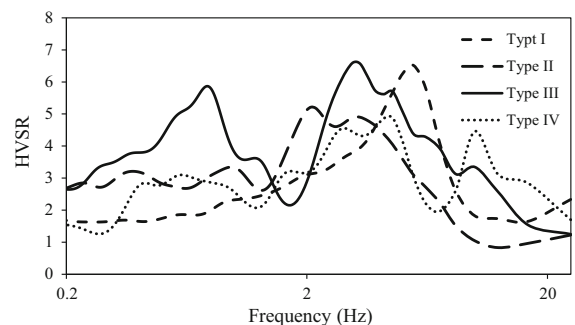

Figure 8
Classification of average HVSR curves into Type I, Type II, Type III and Type IV

and is the first attempt of its kind. Work attempted by Rao et al. (2011) consisted of both subsoil data as well as recorded ground motion to validate the modal characteristics. Present work, however, consists of ground motions records alone at each of the recording stations with no borehole information available. Thus, commenting on depositional mode at each of the recording stations is not possible at this stage. However, if borehole data is available, similar to the work by Rao et al. (2011), above observations at the recording stations can be validated in the future.

9. Conclusion

The present study clearly identifies the problems in the SC given in PESMOS, which are based on surface geology alone. Using ground motion records from recording stations with incorrect SC may lead to erroneous outcomes. In the present work, SC of 90 recording stations located in the western Himalayas and its adjoining areas are attempted. Average HVSR curve at each of the recording station is used to determine f_{peak} value and thus the SC. Based on the present analysis, SC are attempted for all the 90 recording stations following the same classification system used by PESMOS. Present work, however, concludes a variation in the SC for number of recording stations in comparison to present SC as given by PESMOS. Comparison of original and revised SC following Borcherdt (1994) classification scheme is presented from this work. In addition, SC determinations for all the recording stations are done following worldwide followed NEHRP classification scheme. The average HVSR curve used for the above classification are closely matching with the average HVSR curve existing in the literature and proposed for other regions. This enhances the confidence that the outcomes from the present work are correct. Existing literature also supports that based on the modal characteristics of average HVSR curve alone, information about the subsoil characteristics can be assessed. Following this finding, all the average HVSR curves in this work are found belonging to four types. However, in situ subsoil information for each recording station if available in the future, can be used to validate this finding.

Revised SC as well as NEHRP based SC proposed in this work may be very useful in deriving soil response for various SCs. In addition, knowing the SC at each station will be very helpful for deconvolution of recorded ground motions to arrive at bedrock motion at the reference site which can be used in any site response analysis.

Acknowledgements

REFERENCES

Ambraseys, N. N., & Douglas, J. (2004). Magnitude calibration of North Indian earthquakes. *Geophysical Journal International, 159,* 165–206.

Anbazhagan, P., Kumar, A., & Sitharam, T.G. (2011). Amplification factor from intensity map and site response analysis for the soil sites during 1999 Chamoli earthquake. In *Proceedings of the 3rd Indian Young geotechnical engineers conference* (pp. 311–316). New Delhi.

Anbazhagan, P., Kumar, A., & Sitharam, T. G. (2013). Ground motion prediction equation considering combined dataset of recorded and simulated ground motions. *Soil Dynamics and Earthquake Engineering, 53,* 92–108.

Apostolidis, P. I., Raptakis, D. G., Pandi, K. K., Manakou, M. V., & Pitilakis, K. D. (2006). Definition of subsoil structure and preliminary ground response in Aigion city (Greece) using microtremor and earthquakes. *Soil Dynamics and Earthquake Engineering, 26*(10), 922–940.

Ashford, S.A., Warrasak, J., & Panitan, L. (2000). Amplification of earthquake ground motions in Bangkok. In *Proceedings of 12th World Conference on Earthquake Engineering* 1466.

Avouac, J. P., Ayoub, F., Leprince, S., Konca, O., & Helmberger, D. V. (2006). The 2005, M w 7.6 Kashmir earthquake: Sub-pixel correlation of ASTER images and seismic waveforms analysis. *Earth and Planetary Science Letters, 249*(3), 514–528.

Banerjee, S., & Kumar, A. (2017a). Determination of seismic wave attenuation for the Garhwal Himalayas, India. *Geosciences Research, 2*(2), 105–126. doi:10.22606/gr.2017.22005.

Banerjee, S., & Kumar, A. (2017b). Determination of S and Coda Wave attenuation in selected regions of lower and northern Assam within North Eastern India. *Indian Geotechnical Journal.* doi:10.1007/s40098-017-0259-1.

Borcherdt, R. D. (1994). Estimates of site-dependent response spectra for design (methodology and justification). *Earthquake Spectra, 10,* 617–653.

BSSC (2003). Building Seismic Safety Council, NEHRP recommended provisions for seismic regulations for new buildings and other structures. Report FEMA-450 (Provisions), Federal Emergency Management Agency (FEMA), Washington.

EPRI (1993). Guidelines for determining design basis ground motion. Palo Alto, CA: Electric Power Research Institute, 1, EPRI TR-102293.

Guéguen, P., Chatelain, J. L., Guillier, B., & Yepes, H. (2000). An indication of the soil topmost layer response in Quito (Ecuador) using noise H/V spectral ratio. *Soil Dynamics and Earthquake Engineering, 19,* 127–133. doi:10.1016/S0267-7261.

Harbindu, A., Gupta, S., & Sharma, M. L. (2014). Earthquake ground motion predictive equations for Garhwal Himalaya, India. *Soil Dynamics and Earthquake Engineering, 66,* 135–148.

Harinarayan, N. H., & Kumar, A. (2017). Site classification of the strong motion stations of Uttarakhand, India, Based on the model horizontal to vertical spectral ratio. In *Proceedings of geotechnical frontiers*, GSP 281, Orlando: Florida (ASCE special Publication).

IBC (2009) International Building code, International Building Council, Washington.

Iyengar, R. N., & Ghosh, S. (2004). Seismic hazard mapping of Delhi city. In *13th world conference on earthquake engineering*, Vancouver. Paper No. 180.

Kayal, J. R. (1996). Precursor seismicity, foreshocks and aftershocks of the Uttarkashi earthquake of October 20, 1991 at Garhwal Himalaya. *Tectonophysics, 263,* 339–345.

Konno, K., & Ohmachi, T. (1998). Ground motion characteristics estimated from spectral ratio between horizontal and vertical components of microtremor. *Bull Seism Soc Am, 88*(1), 228–241.

Kramer, S. L. (1996). Geotechnical earthquake engineering. *Engineering, 6,* 653.

Krinitzsky, E. L., & Hynes, M. E. (2002). The Bhuj, India, earthquake: Lessons learned for earthquake safety of dams on alluvium. *Engineering Geology, 66,* 163–196.

Kumar, A., & Baro, O. (2016). In-direct estimation of local soil response in the light of past as well as recent earthquakes in the Shillong Plateau. In: *Proceeding of the Indian Geotechnical Conference IIT Madras*, Chennai.

Kumar, A., Baro, O., & Harinarayan, N. H. (2016). Obtaining the surface PGA from site response analyses based on globally recorded ground motions and matching with the codal provisions. *Natural Hazards, 81,* 543–572.

Kumar, A., Harinarayan, N. H., & Baro, O. (2015). High amplification factor for low amplitude ground motions: Assessment for Delhi. *Disaster Advances, 8*(12), 1–15.

Kumar, A., Harinarayan, N.H, & Baro O. (2017a), Effects of earthquake motion and overburden thickness on strain behavior of clay and sandy soils. In *Proceedings of 16th World Conference on Earthquake Engineering*. 9–13 January, Santiago: Chile.

Kumar, A., Harinarayan, N. H., & Baro, O. (2017b). Nonlinear soil response to ground motions during different earthquakes in Nepal, to arrive at surface response spectra. *Natural Hazards.* doi:10.1007/s11069-017-2751-4.

Kumar, A., Mittal, H., Sachdeva, R., & Kumar, A. (2012). Indian strong motion instrumentation network. *Seismological Research Letters, 83*(1), 59–66.

Kumar, A., & Mondal, J. K. (2017). Newly developed MATLAB based code for equivalent linear site response analysis. *Geotechnical and Geological Engineering*, 1–23.

Lee, V. W., & Trifunac, M. D. (2010). Should average shear-wave velocity in the top 30 m of soil be used to describe seismic amplification? *Soil Dynamics and Earthquake Engineering, 30,* 1250–1258.

Luzi, L., Puglia, R., Pacor, F., Gallipoli, M. R., Bindi, D., & Mucciarelli, M. (2011). Proposal for a soil classification based on parameters alternative or complementary to V_{s30}. *Bulletin of the Seismological Society of America, 9*(6), 1877–1898.

Mahajan, A. K., Galiana-Merino, J. J., Lindholm, C., Arora, B. R., Mundepi, A. K., Rai, N., et al. (2011). Characterization of the sedimentary cover at the Himalayan foothills using active and passive seismic techniques. *Journal of Applied Geophysics, 73*(3), 196–206.

Mahajan, A. K., Gupta, V., & Thakur, V. C. (2012). Macroseismic field observations of 18 September 2011 Sikkim earthquake. *Natural Hazards, 63,* 589–603.

Mahajan, A. K., & Kumar, S. K. (2004). Macroseismic field observations of January 26th, 2001 Kachchh earthquake and its seismotectonics. *Journal of Asian Earth Sciences, 23,* 17–23.

Martin, A. J., & Diehl. J. G. (2004). Practical experience using a simplified procedure to measure average shear_wave velocity to a depth of 30 meters (Vs30). In *13th World Conference on Earthquake Engineering*, Vancouver, Canada. Paper no. 952

Mirzaoglu, M., & Dýkmen, U. (2003). Application of microtremors to seismic microzoning procedure. *Journal of the Balkan Geophysical Society, 6*(3), 143–156.

Mittal, H., Kamal, Kumar A., & Singh, S. K. (2013). Estimation of site effects in Delhi using standard spectral ratio. *Soil Dynamics and Earthquake Engineering, 50,* 53–61.

Mittal, H., Kumar, A., & Ramhmachhuani, R. (2012). Indian national strong motion instrumentation network and site characterization of its stations. *International Journal of Geosciences, 3*(06), 1151.

Mohamed, A. M. E., Hafiez, H. E. A., & Taha, M. A. (2013). Estimating the near-surface site response to mitigate earthquake disasters at the October 6th city, Egypt, using HVSR and seismic techniques. *NRIAG Journal of Astronomy and Geophysics, 2,* 146–165.

Mondal, J. K., & Kumar, A. (2016). Impact of higher frequency content of input motion upon equivalent linear site response analysis for the study area of Delhi. *Geotechnical and Geological Engineering, 35*(3), 959–981.

Mugnier, J. L., Gajurel, A., Huyghe, P., Jayangondaperumal, R., Jouanne, F., & Upreti, B. (2013). Structural interpretation of the great earthquakes of the last millennium in the central Himalaya. *Earth Science Reviews, 127,* 30–47.

Mundepi, A. K. (2013). Seismic microzonation study in Doon Valley, Northwest Himalaya, India. *Journal of the Geological Society of India, 81,* 767–773.

Nakamura, Y. (1989). *A method for dynamic characteristics estimation of subsurface using microtremor on the ground surface*. Railway Technical Research Institute, Quarterly Reports, 30(1).

Ni, J., & Barazangi, M. (1984). Seismotectonics of the Himalayan Collision Zone: Geometry of the underthrusting Indian Plate beneath the Himalaya. *Journal of Geophysical Research, 89,* 1147–1163.

Pandey, B., Jakka, R. S., & Kumar, A. (2016). Influence of local site conditions on strong ground motion characteristics at Tarai region of Uttarakhand, India. *Natural Hazards, 81,* 1073–1089.

Park D., & Hashash, Y. M. (2004). Probabilistic seismic hazard analysis with nonlinear site effects in the Mississippi embayment. In: *Proceedings of the 13th world conference on earthquake engineering*, Vancouver, Paper No. 1549.

Paudyal, Y. R., Yatabe, R., Bhandary, N. P. & Dahal, R. K. (2012). A study of local amplification effect of soil layers on ground motion in the Kathmandu Valley using microtremor analysis. *Earthquake Engineering and Engineering Vibration*, *11*(2), 257–268.

Philip, G., Suresh, N., & Bhakuni, S. S. (2014). Active tectonics in the northwestern outer Himalaya: evidence of large-magnitude palaeoearthquakes in Pinjaur Dun and the Frontal Himalaya. *Current Science, 106,* 211–222.

Rao, P., Kumar, R., Seshunarayana, M., Shukla, T., Suresh, A. K., Pandey, G., et al. (2011). Site amplification studies towards seismic microzonation in Jabalpur urban area, central India. *Physics and Chemistry of the Earth, 36,* 1247–1258.

Sarkar, I., Pachauri, A. K., & Israil, M. (2001). On the damage caused by the Chamoli earthquake of 29 March, 1999. *Journal of Asian Earth Sciences, 19,* 129–134.

Sharma, M. L., Narayan, J. P., & Rao, K. S. (2004). Seismic microzonation of Delhi region in India. In *Proceedings of 13th World Conference on Earthquake Engineering (13WCEE)*. (Paper no. 2043).

Sharma, J., Chopra, S., & Roy, K. S. (2014). Estimation of source parameters, quality factor (QS), and site characteristics using accelerograms: Uttarakhand Himalaya region. *Bulletin of the Seismological Society of America*, *4*(1), 360–380.

Srivastava, H. N., Bansal, B. K., & Verma, M. (2013). Largest earthquake in Himalaya: An appraisal. *Journal of the Geological Society of India, 82,* 15–22.

Stephenson, W. R. (2007). HVSR, SSR, and V_{S30} values at three New Zealand Basin Arrays. *Journal of Earthquake Engineering, 11,* 987–1009.

Theodulidis, N. P., & Bard, P. Y. (1995). Horizontal to vertical spectral ratio and geological conditions: an analysis of strong motion data from Greece and Taiwan (SMART-1). *Soil Dynamics and Earthquake Engineering, 14*(3), 177–197.

Verma, M., Singh, R. J., & Bansal, B. K. (2014). Soft sediments and damage pattern: a few case studies from large Indian earthquakes Vis-A-Vis seismic risk evaluation. *Natural Hazards, 74,* 1829–1851.

Walling, M. Y., Mohanty, W. K., Nath, S. K., Mitra, S., & John, A. (2009). Microtremor survey in Talchir, India to ascertain its basin characteristics in terms of predominant frequency by Nakamura's ratio technique. *Engineering Geology, 106,* 123–132.

Yamazaki, F., & Ansary, M. A. (1997). Horizontal-to-vertical spectrum ratio of earthquake ground motion for site characterization. *Earthquake Engineering and Structural Dynamics, 26*(7), 671–689.

Zhao, J. X., Irikura, K., Zhang, J., Fukushima, Y., Somerville, P. G., Asano, A., et al. (2006). An empirical site-classification method for strong-motion stations in Japan using H/V response spectral ratio. *Bulletin of the Seismological Society of America, 96,* 914–925.